Guide to
the Realization of the ITS-90

Cryogenic Fixed Points

Cryogenic Fixed Points

CONTENTS

Last updated 1 January 2018

Guide to the Realization of the ITS-90

Cryogenic Fixed Points

B Fellmuth, Physikalisch-Technische Bundesanstalt, Berlin, Germany

E Mendez-Lango, Centro Nacional de Metrologia, Queretaro, Mexico

T Nakano, National Metrology Institute of Japan, AIST, Ibaraki, Japan

F Sparasci, Laboratoire National de Métrologie et d'Essais - Cnam, Paris, France

Abstract

This paper is a part of guidelines, prepared on behalf of the Consultative Committee for Thermometry, on the methods for how to realize the International Temperature Scale of 1990 (ITS-90).

It describes ways of realizing the defining fixed points of the ITS-90 which comprise triple points of cryogenic gases to be used for the calibration of interpolation instruments.

1   INTRODUCTION

In this section, the realization of the triple points of cryogenic gases as defining fixed points of the ITS-90 is treated independently of the realization of metal fixed points for contact thermometry, which is discussed in ITS-90 Guide Section 2.4 *Metal Fixed Points for Contact Thermometry*, above all because of the special properties of the cryogenic gases as fixed-point substances. The thermal conductivity and the heat of fusion of a cryogenic gas are orders of magnitude smaller than those of a metal.

Six cryogenic gas fixed points are specified in the ITS-90: triple points of equilibrium hydrogen, neon, oxygen and argon as well as two vapour-pressure points of equilibrium hydrogen. (Best estimates of the deviation of the ITS-90 fixed-point temperatures from thermodynamic values are given in an appendix of the *MeP*-K [CCT 2010, Fischer *et al.* 2011].) All six cryogenic fixed points are used for the calibration of capsule-type standard platinum resistance thermometers, see ITS-90 Guide Chapter 5 *Platinum Resistance Thermometry*. Two of them (triple point of oxygen rarely and triple point of argon) are applied for calibrations of long-stem standard platinum resistance thermometers. (In all cases, the thermometers have also to be calibrated at the triple point of mercury, which is not a cryogenic fixed point in the narrow sense and treated in ITS-90 Guide Section 2.4 *Metal Fixed Points for Contact Thermometry*.) Two others (triple points of hydrogen and neon) are two of the three points used for calibrations of interpolating constant-volume gas thermometers, see ITS-90 Guide Chapter 4 *Gas Thermometry*. Some properties of the four fixed-point substances are given in Table 1.

Conveniently, the triple-point temperatures of the cryogenic gases are affected by only a limited number of impurities, distinct for each fixed-point substance, see ITS-90 Guide Section 2.1 *Influence of Impurities*. Unfortunately, the influence of the isotopic composition is very large for hydrogen and neon, see the Technical Annex of the *mise en pratique* of the definition of the kelvin (*MeP*-K) [Fellmuth *et al.* 2016, http://www.bipm.org/en/publications/mep_kelvin/]. The Technical Annex is mandatory for the realization of the ITS-90. This annex specifies the isotopic composition of hydrogen and neon. Such a specification is not included in the scale definition itself.

Between the triple points of hydrogen and neon, the sensitivity of platinum resistance thermometers is extremely small. Therefore, mostly rhodium-iron resistance thermometers are used. For their calibration, the realization of the ITS-90 in this temperature range and below is performed applying the interpolating gas thermometer, i.e. the two boiling points of equilibrium hydrogen are rarely utilised. These two fixed points are not dealt with in this section mainly because their realization can be performed following the recommendations given in ITS-90 Guide Chapter 3 *Vapour Pressure Scales and Pressure Measurements* on the realization of the helium vapour-pressure scales. Equations (11a) and (11b) in the text of the ITS-90 [Preston-Thomas 1990] are the necessary vapour-pressure-temperature relations of equilibrium hydrogen, which are valid in two narrow temperature ranges (17.025 K to 17.045 K and 20.26 K to 20.28 K, respectively).

There is only one special problem in realizing the two hydrogen points, cf. Guide Chapter 3: The vapour-pressure temperature may depend on whether gas has been removed from or added to the sample chamber because of isotopic composition effects. Isotope fractionation may result in a temperature difference of 0.4 mK between the dew point (vanishingly small liquid fraction) and the boiling point (vanishingly small vapour fraction). In practice, the boiling point is used since the catalytic action is more efficient if the free liquid is in contact with the catalyst, which is necessary to ensure that the hydrogen has the equilibrium composition of the two nuclear-spin isomers, see below.

Table 1. Properties of the four cryogenic gases equilibrium hydrogen, neon, oxygen and argon at their triple points: T_{90} assigned fixed-point temperature; p pressure; Q_{HF} heat of fusion; c_{Cu} specific heat of copper at constant pressure (Q_{HF}/c_{Cu} is a measure of the ability of the melting substance to maintain a mass of construction material copper at the triple point); $A = Q_{HF} / (R \ (T_{90})^2)$ cryoscopic constant (R molar gas constant); dT_{90}/dp temperature variation with pressure; dT_{90}/dl temperature variation with depth; λ_l thermal conductivity of the liquid; ρ_l and ρ_s density of liquid and solid, respectively; c_s specific heat of the solid.

Substance	Hydrogen	Neon	Oxygen	Argon
T_{90} / K	13.8033	24.5561	54.3584	83.8058
p / kPa	7.034	43.379	0.1464	68.892
Q_{HF} / (J / mol)	117	335	444	1188
Q_{HF} / c_{Cu}	90	33	4.4	6
A / K^{-1}	0.0739	0.0668	0.0181	0.0203
A^{-1} / (μK / 10^{-6} mole fractions)	14	15	55	49
dT_{90}/dp (10^{-8} K / Pa)	34	16	12	25
dT_{90}/dl (10^{-3} K / m)	0.25	1.9	1.5	3.3
λ_l / (W / (Km))	0.103	0.117	0.196	0.125
ρ_l (g / L)	71	1206	1141	1392
ρ_s (g / L)	87	1444	1351	1623
c_s (J / (K mol))	6.2	24.3	46	33.2

2 CRYOGENIC TRIPLE-POINT SYSTEMS

2.1 Triple-point cells

Triple-point systems have the great advantage over boiling-point systems of requiring no pressure measurements. Cryogenic triple points are almost always obtained from melting rather from freezing of the sample, mainly because controlled electrical heating is more easily performed than cooling. A cryogenic triple-point cell may be refillable, via a more-or-less-permanently connected gas handling and purifying system, or it may be a more robust, permanently sealed unit. The latter type is now almost universally used for triple-point realizations. Sealed cells can be better thermally isolated, because no metallic filling tube is necessary, can be used for many years, even decades, and can be transported as transfer standards.

Sealed cells for capsule-type thermometers have been developed since the mid-seventies of the last century [Bonnier and Malassis 1975, Pavese *et al.* 1976 and 1978]. They all consist of a volume of gas at high pressure (at room temperature) sealed in a small copper or stainless steel container. On cooling, the gas condenses as liquid and then solid, occupying only a small part of the volume. The design must allow the standard platinum resistance thermometers to make good contact with the sample, so that it quickly responds to the temperature of the solid-liquid interface during melting.
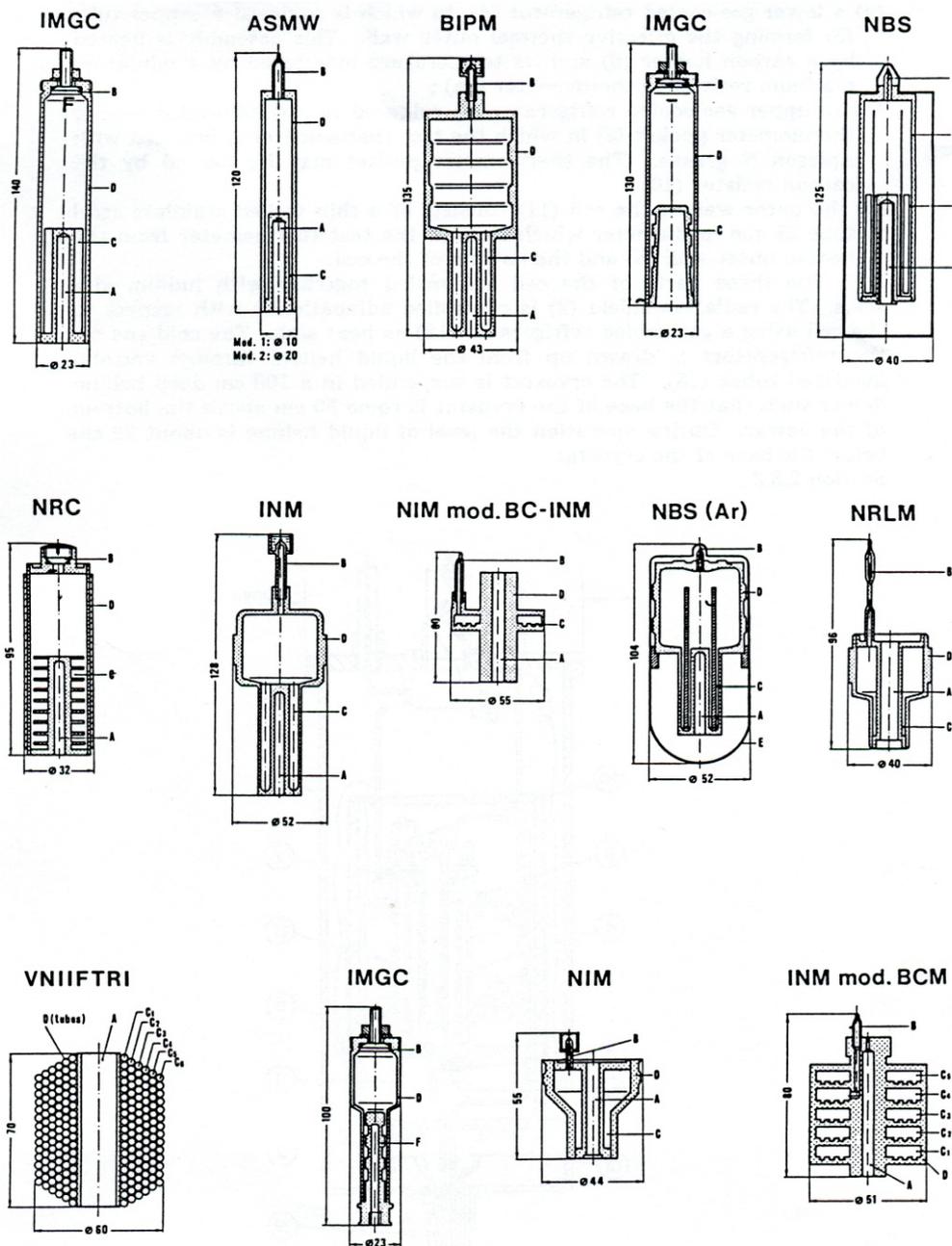
Figure 1. A selection of designs for sealed all-metal triple-point cells included in a first international intercomparison of fixed points (dimensions are in mm) [Pavese *et al.* 1984, Pavese 1984]. © Bureau International des Poids et Mesures. Reproduced by permission of IOP Publishing. All rights reserved.

Such cells were initially used for a trilateral intercomparison [Ancsin 1978]. A first international intercomparison of fixed points by means of sealed cells was made shortly afterwards [Pavese *et al.* 1984, Pavese 1984]. In this intercomparison, cells for capsule-type thermometers of a wide variety of successful designs were included, see Figure 1. Later, special modular multi-compartment cells were developed within the framework of an international collaboration [Pavese *et al.* 2003a and 2003b, Hermier *et al.* 2003]. Two lines of cell design, see Figures 2 and 3, yielded a nearly equal

improvement of the fixed-point realization. The multi-compartment cells allow thermometers to be calibrated more efficiently at several fixed points in one low-temperature run. They were included in a second international intercomparison, in which it was possible to compare the parameters of all modern cell designs, see [Fellmuth *et al.* 2012]. The references cited therein give information on the designs and filling technologies. A new design of multi-well single cells is described in [Nakano *et al.* 2007] and shown in Figure 4. Other new designs can be seen in Section 2.4.3.1 of [Pavese and Molinar Min Beciet 2013].
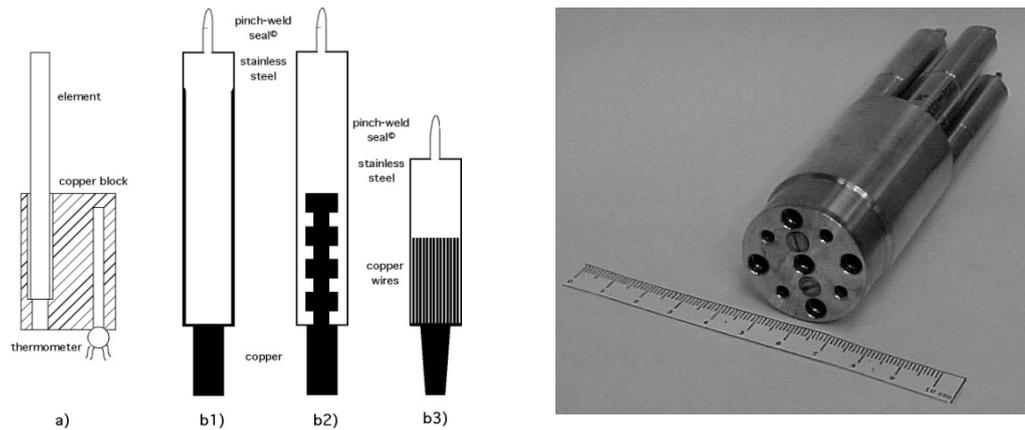
Figure 2. Sealed-cell models developed at INRIM after 1990 within the framework of an international collaboration, reproduced from [Pavese *et al.* 2003a and 2003b] with the permission of AIP Publishing: On the left (not to scale): Schematic diagrams: a) Copper block for several cells and thermometers, b) Cells, each filled with a single substance: b1) model A, with copper internal wall, b2) model B, with internal copper body, b3) model C, with internal wireframe-copper body. On the right: Photograph of a copper block with four cells.
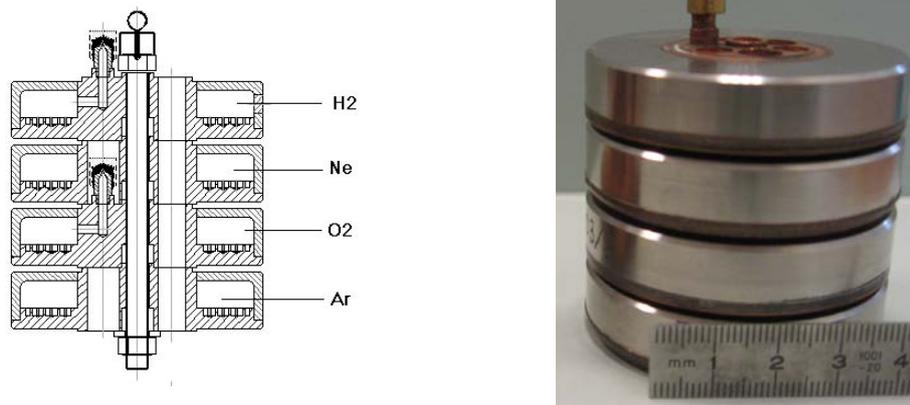
Figure 3. Sealed-cell model developed at LNE-Cnam after 1990 within the framework of an international collaboration, reproduced from [Hermier *et al.* 2003, Pavese *et al.* 2003a] with the permission of AIP Publishing: On the left (not to scale): Schematic diagram of an assembly composed of four cells for the realization of the triple points of hydrogen, neon, oxygen, and argon, pressed together with the central screw. On the right: Photograph of an assembly with four cells.
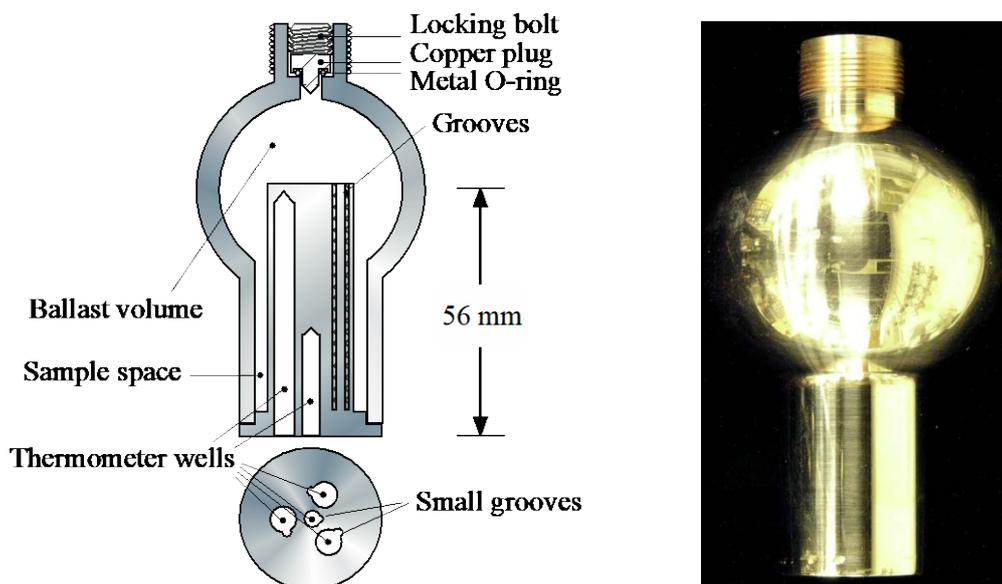
Figure 4. Single sealed multi-well triple-point cell of new generation developed at NMIJ/AIST [Nakano *et al.* 2007 – illustration reproduced with permission of Springer]: On the left: Schematic diagram: The material is oxygen-free high-conductivity copper. In order to ensure cleanliness of the inside of the cell, all of its parts have been subjected to chemical polishing. Three reentrant wells are provided for capsule-type standard platinum resistance thermometers or rhodium-iron resistance thermometers. The middle of the copper block also contains a reentrant well for a control thermometer. Each thermometer well has a small lateral hollow for application of grease to enhance the thermal contact and for easy evacuation of residual gas from the space around the installed thermometer. Internally, grooves for ensuring good thermal contact with the solid and/or liquid phases of the substance are provided around the copper thermometer block. The sealing device of the multi-well model is a metal O-ring made of stainless steel [Nakano *et al.* 2003]. On the right: Photograph without thermometers [photograph reproduced on the courtesy from T. Nakano (NMIJ/AIST)].

Sealed triple-point cells for long-stem thermometers are similar in principle both in design and in operation to those for capsule-type thermometers, but are much longer so as to provide adequate immersion for the thermometer. The necessary thermometer well compromises the isothermal condition. For details of their design and operation see [Bonnier 1975 and 1987, Ancsin and Phillips 1976, Bloembergen *et al.* 1990, Furukawa 1992, Pond 2003, Ding *et al.* 2011 and 2012, Didi-Alaoui *et al.* 2013] and Figure 5.
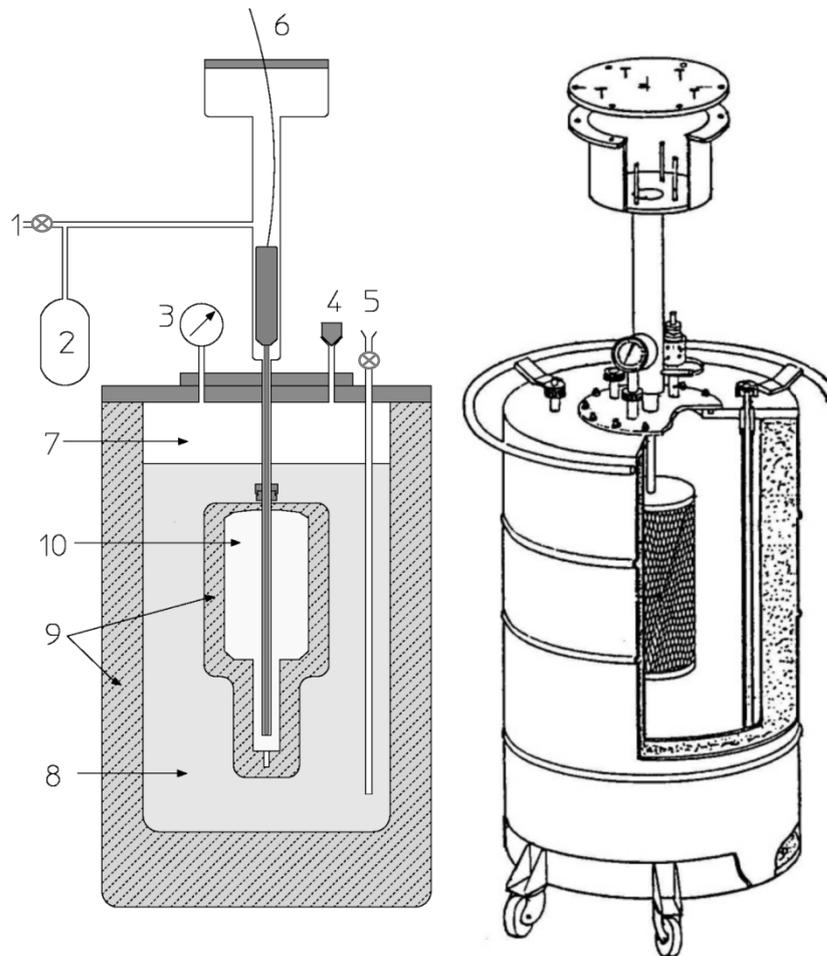
Figure 5. First commercial apparatus for the calibration of long-stem standard platinum resistance thermometers at the triple point of argon using a sealed cell developed at LNE/Cnam: On the left: Schematic diagram [on the courtesy from F. Sparasci (LNE-Cnam)]: 1 helium exchange-gas inlet, 2 helium reservoir (balloon), 3 manometer, 4 pressure-control valve, 5 filling tube for liquid nitrogen, 6 thermometer well, 7 nitrogen vapour, 8 bath of liquid nitrogen, 9 thermal isolation (polyurethane foam), 10 stainless-steel cell with argon. On the right: Scheme with cut-out [Hermier *et al.* 2005].

All sealed triple-point cells must be designed to withstand the pressure arising at the maximum expected temperature (typical room-temperature pressures range from 0.5 MPa to 20 MPa). The heat capacity of the container is not directly of great importance in determining melting curves. It would be important if freezing curves were measured, because of the effects of supercooling. But supercooling may also have an influence on the melting curve especially for argon, see below, because depending on the heat capacity and the supercooling temperature, a large portion of the sample may freeze very quickly during recalescence, resulting in a strong distortion of the crystal lattice of the solid. For cells for long-stem thermometers in particular there is also the problem that a significant fraction of the sample may condense on the walls or roof of the cell, and not in the sample space. There may also be migration of the sample by sublimation and condensation on any cold spots. By contrast, open cells do not need a gas expansion volume, so can be both smaller and contain a

larger sample of the substance. They do not have to be particularly robust and, thus, may be designed to have a heat capacity substantially less than that of a sealed cell of comparable sample size.

The cell design should be such as to reduce as much as possible the thermal resistance between the sample and the thermometer, taking due account of the very low thermal conductivities of liquid gases. Preferably, the thermometer is surrounded by the sample (within the heat sink) rather than located between the heat sink and parasitic heat sources [Ancsin 1973a]. Heat conduction to the sample can be made sufficiently good, either by subdividing the chamber by a set of copper baffles [Ancsin 1973b], by increasing the contact surface by optimised grooves in the inner chamber wall [Hermier *et al.* 2003, Nakano *et al.* 2007] or even by using a bunch of OFHC copper wires [Pavese *et al.* 2003b]. On the other hand, the construction should not be too complicated because a thorough cleaning of the inside of the cell should be possible.

For filling the cells, high-purity gas-handling systems composed of ultra-high vacuum components have to be used. This is necessary in order to be able to remove the air that initially forms several layers on all inner surfaces and to manipulate the ultra-pure gases (with total impurity concentrations of order one part per million, at the best level) without introducing any extra impurities. Impurities introduced during the filling would cause permanent problems because the impurity content cannot be checked after the sealing, and any outgassing of the inner cell walls would limit the long-term stability. (On the basis of the measurement of outgassing rates, it is concluded in [Liu *et al.* 1992] that well-prepared sealed cells may be stable within 0.1 mK for more than 13 years.) For checking purposes, a gas-handling system should incorporate a residual gas analyser as an essential component. The seal of a cell must remain leak-proof for an indefinitely long time. A variety of means and techniques have been successfully used (cf. Section 2.4.3.1 *Sealed Cells for Capsule Thermometer* in [Pavese and Molinar Min Beciet 2013]): indium gasket fitted inside or outside the cell; pinched copper tube, then soft soldered for mechanical protection; stainless-steel tube pinched with a gold wire inside; pinch-weld stainless-steel tube.

A special problem in realizing the triple point of hydrogen is the existence of two nuclear-spin isomers (often designated by the prefixes *ortho* and *para*). The equilibrium ortho-para composition is temperature dependent. On liquefaction the composition changes slowly with time and there are corresponding changes in the physical properties. In particular the difference between the fixed-point temperatures of normal hydrogen, which has the room-temperature composition, and equilibrium hydrogen is of order 0.1 K, i.e. three orders of magnitude larger than the best realization uncertainty. For achieving the equilibrium composition in acceptable time, a suitable catalyst has to be placed in the sample chamber. The materials most commonly employed for this purpose have been transition metal oxides and rare-earth oxides, see the detailed discussion in [Fellmuth *et al.* 2005]. The catalyst may be of course a source of impurity. Furthermore, it has to be considered that all catalysts for *ortho-para* conversion are chemically active and an activation may be necessary.
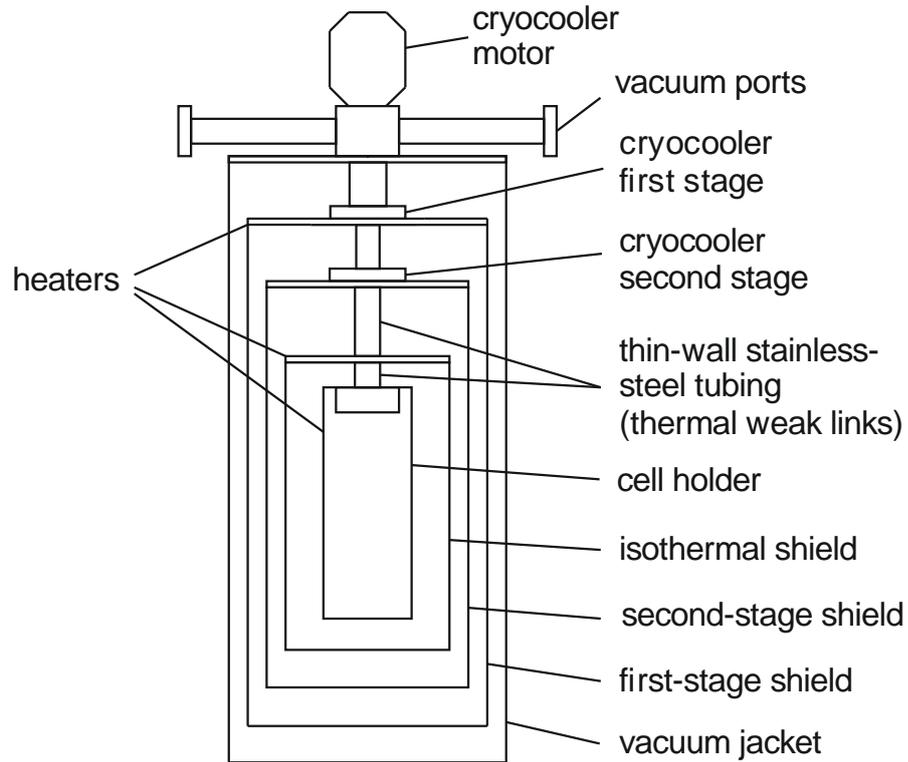
2.2　Cryogenic equipments

In order to keep temperature gradients low, heat flows in the sealed triple-point cell must be extremely small, i.e. isothermal conditions are necessary. To this end, the cell is surrounded by one or more temperature-controlled heat shields, the whole being enclosed in a vacuum jacket for thermal isolation. The cell is further thermally isolated by suspending it using non-metallic threads, e.g. nylon threads, or thin stainless-steel wires. Traditionally the vacuum jacket was normally immersed in the cryogenic fluid of a liquid-refrigerant cryostat. Several such triple-point cryostats have been described [Ancsin and Phillips 1969, Ancsin 1970, Pavese 1978, Compton and Ward 1976, Kemp *et al.* 1976]. One of these is illustrated in Figure 6. Nowadays preferably cryostats designed around closed-cycle cryocoolers are applied for the realization of cryogenic fixed points. Examples of modern systems are given in [Steele 1997, Hill and Steele 2003, Sakurai 2003, Nakano *et al.* 2007, Pavese *et al.* 2011, Sparasci *et al.* 2011, Yang *et al.* 2011, Pavese and Molinar Min Beciet 2013]. The basic design of such cryostats, which make it easier to realize isothermal conditions, is illustrated in Figure 7. As a collateral effect, these cryostats allow measurements to be performed for extremely long periods (months), uninterrupted by disturbances usually caused by refilling liquid refrigerant.
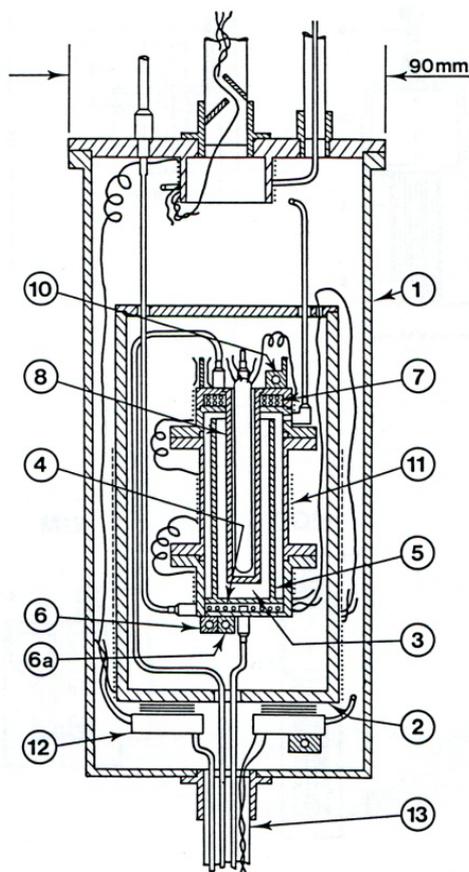
Figure 6. Schematic diagram of a cryostat with an open cell for the realization of boiling and triple points of cryogenic gases [Kemp *et al.* 1976] © Bureau International des Poids et Mesures. Reproduced by permission of IOP Publishing. All rights reserved. (A similar system can be used for measurements with sealed cells.) Isothermal conditions for the cell are generated by vacuum isolation and a temperature-controlled isothermal radiation shield. In the diagram, the numbers mark the following parts: (1) the outer vacuum case, (2) a temperature-controlled outer shield and (3) the cell containing the fixed-point sample. The cell consists of three parts:

a)   A lower gas-cooled refrigerator (4), to which is soldered a copper tube (5) forming the effective thermal outer wall. This assembly is heated by a carbon heater (6) and its temperature monitored by a miniature platinum resistance thermometer (6a);

b)   An upper gas-cooled refrigerator (7) soldered to a thick-walled copper thermometer pocket (8) in which the test thermometer is inserted with grease. The thermometer pocket may be heated by the carbon resistor (10);

c)   The outer wall of the cell (11) consists of a thin-walled stainless steel tube 25 mm in diameter which isolates the test thermometer from the heated outer wall (5) and the bottom of the cell.

The three parts of the cell are sealed together with indium-wire seals. The radiation shield (2) is controlled isothermally with respect to the cell using a gas-cooled refrigerator (12) as heat sink. The cold gas for the refrigerators is drawn up from the liquid helium through vacuum-insulated tubes (13). The cryostat is suspended in a 100 cm deep helium dewar such that the base of the cryostat is some 50 cm above the bottom of the dewar. During operation the level of liquid helium is about 20 cm below the base of the cryostat.

cryocooler
motor

vacuum ports

cryocooler
first stage

cryocooler
second stage

thin-wall stainless-
steel tubing
(thermal weak links)

heaters

cell holder

isothermal shield

second-stage shield

first-stage shield

vacuum jacket

Figure 7. Schematic diagram of a cryostat constructed around a two-stage closed-cycle cryocooler. A vacuum jacket surrounds the assembly to provide the basic thermal isolation from the room temperature environment. Concentric copper shields are attached to both stages of the cryocooler. Isothermal conditions are generated by controlling the temperature of the isothermal shield with respect to the cell temperature such that the parasitic heat load to the cell and thus the static temperature-measurement error is sufficiently small, see text. [illustration reproduced on the courtesy from B. Fellmuth (PTB)].

3 REALIZATION OF A CRYOGENIC TRIPLE POINT

3.1 Measurement protocol

For fixed-point realizations, the temperature of the solid-liquid interface is the fixed-point temperature and must be measured as accurately as possible. Due to the very small thermal conductivity of the cryogenic gases, it is not possible to heat the fixed-point sample continuously through the solid-to-liquid phase transition. Continuous heating would cause large temperature gradients, which are usually dominated by the liquid phase. (Additional thermal resistances exist between the different parts of a cell [Wolber and Fellmuth 2011].) Instead the calorimetric method has to be applied, see for instance [Pavese *et al.* 2003a, Fellmuth *et al.* 2005] and the references cited therein. The sample is heated through the phase transition under nearly isothermal conditions by the intermittent input of heat. After each heat pulse, the cell is allowed to come to thermal equilibrium. The calorimetric method is illustrated in Figure 8.
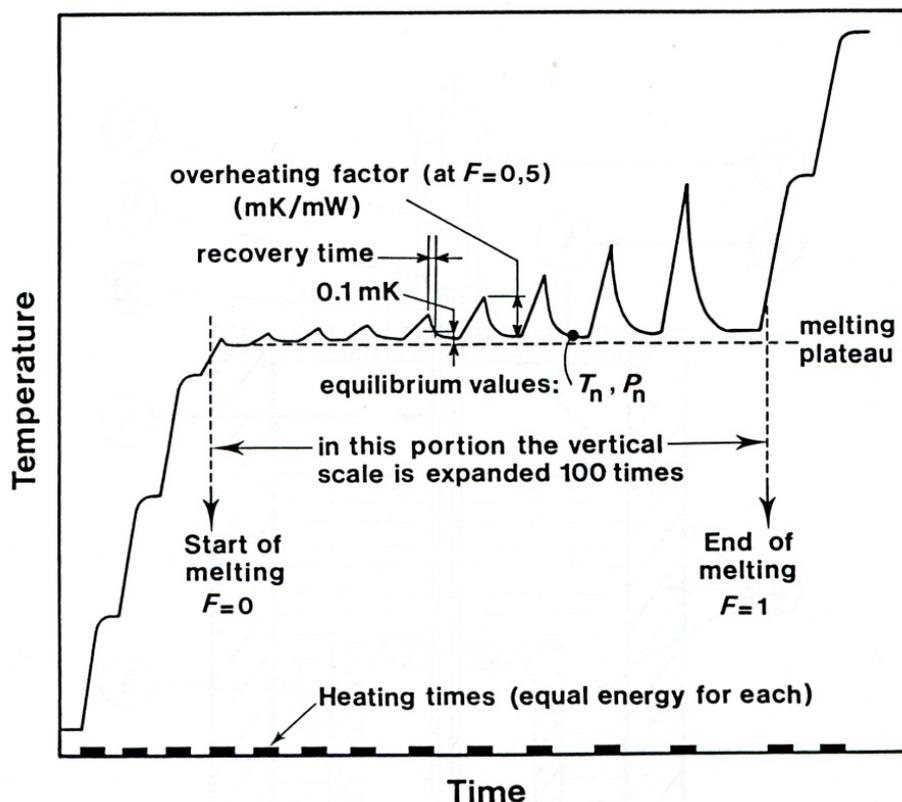
Figure 8. A schematic representation of melting a fixed-point sample by intermittent heating (after Pavese (1984)). Heating is supplied in equal-energy steps. *F* is the melted fraction. The melting lasts at least several hours.

A plot (or least-squares analysis) of the equilibrium temperatures as a function of the fraction *F* of the sample melted gives a well-defined representation of the melting curve. (For determining *F*, the heat of fusion Q_{HF} of the fixed-point sample is needed. For measuring Q_{HF}, it is recommended to heat the sample through the solid-to-liquid phase transition applying two short heat pulses and

allowing the sealed triple-point cell assembly to come to thermal equilibrium roughly near the middle of the melting curve, see Appendix 1. Alternatively, Q_{HF} can be calculated from the sum of applied heat and the known parasitic heat load for the duration of the melting-curve measurement. The obtained Q_{HF} value is to be compared with the value expected from the sample amount, when known.) The representation versus $1/F$ is also widely used. Different representations should be checked, in order to determine which representation allows a better separation of the different parts of the melting curve and an approximation of part of the curve with a simple function. Most melting curves plotted versus F consist of a curved region at the onset of melting followed by a flat region over which the bulk of the phase transition occurs, and finally a region of rapid temperature rise as melting is completed. The shape and transition temperature depend on the purity and crystal quality of the sample, on the experimental technique used, and for hydrogen and neon, on isotopic effects. The melting-curve depression at the beginning is suspected to be caused primarily by the influence of crystal defects. The distorted sample parts melt at lower temperatures due to the weakening of the crystal lattice, which results in smaller binding energies. This is called pre-melting. Pre-melting is especially evident with hydrogen for the sample portions in direct contact with the spin-conversion catalyst. A temperature offset may occur, especially towards the end of the melting curve, due to the poor thermal conductivity of the liquid phase. This requires careful estimation of static temperature-measurement errors, see the subsequent subsection. The question of deducing the triple-point temperature from an observed melting curve is discussed in Subsection 3.4.

Usually the melting curves are measured in the F range from 5% to 95%. The measurement at $F = 5\%$ is useful for annealing the sample and for looking for possible pre-melt effects. The equilibrium temperature at $F = 95\%$ is measured to check the thermal conditions. The usually high thermal resistances of the liquid sample portions at $F = 95\%$ make the measurements very sensitive to parasitic heat loads.

Because special techniques have to be applied for the realization of the cryogenic fixed points, a detailed measurement protocol has been developed. The protocol was first suggested in [Fellmuth *et al.* 1999] for the second international intercomparison [Fellmuth *et al.* 2012], recommending the main steps of the investigation of the thermal behaviour of triple-point cells in order to make the results obtained at different institutes comparable. Thermal behaviour means primarily the relationship between the temperature of the solid-liquid interface and the temperature indicated by the thermometers. It was also intended to harmonize the estimation of the measurement uncertainty. Considering the progress described especially in [Pavese *et al.* 2003a and 2003b, Hermier *et al.* 2003, Fellmuth *et al.* 2005 and 2012] and the references cited therein, the protocol was further developed [Wolber and Fellmuth 2013, Fellmuth 2013]. A detailed theoretical foundation of the improved protocol including a model for describing the thermal conditions is given in [Wolber and Fellmuth 2011 and 2013].

The protocol contains recommendations for different aspects of the fixed-point realization, which are explained in this guide in the subsections and appendices given in parentheses: determination of the thermal parameters of the sealed cells and the apparatus (Subsections 3.2 and 3.3), measurement conditions (Subsection 3.2), series of measurements (Appendix 1), recording of data (Appendix 2), establishment of an uncertainty budget (Subsection 4), especially the reliable estimation of static and dynamic temperature-measurement errors (Subsections 3.2 and 3.3). For each fixed-point realization, it is recommended to determine the following parameters: thermal resistance R_{cs} between the metal parts of the cell and the solid-liquid interface, heat capacity C_c of the cell assembly, heat of fusion Q_{HF} of the sample, parasitic heat load to the cell, thermal recovery time constant τ, and recovery periods t_r necessary for decreasing the dynamic temperature-measurement

error ΔT_{dyn} below a desired level ($\Delta T_{dyn} = T_c - T_e$ difference between the measured cell temperature T_c and the equilibrium value T_e).

3.2 Thermal conditions and static temperature-measurement errors

The internal thermal resistance R_{cs} between the metallic body of the cell and the solid phase, which cannot overheat (i.e. acting as a heat sink) during melting, is a crucial parameter for characterizing the thermal conditions. (R_{cs} has been first introduced in [Fellmuth *et al.* 1997]. It is an effective value, see [Wolber and Fellmuth 2011].) R_{cs} is given by the relation

$$R_{cs} = (T_c - T_s) / P_u , \qquad (1)$$

where $\Delta T_{cs} = (T_c - T_s)$ is the temperature difference between the temperature T_c of the metallic cell body measured with a thermometer and the temperature T_s of the solid phase, and P_u is the unbalanced heat load resulting from the summation of heat leaks P_e (exchanged with the environment), dissipation P_m inevitably associated with the measurement itself ("self heating"), and heat input P_h to change the fraction F of sample melted: $P_u = P_e + P_m + P_h$. For a given value of P_u, the static temperature-measurement error amounts to $\Delta T_{stat} = P_u R_{cs}$, which yields, without heating and after correcting for the "self heating", $\Delta T_{stat} = P_e R_{cs}$, i.e. ΔT_{stat} is equal to ΔT_{cs} for P_m and P_h equal to zero. Thus, reliable R_{cs} data are necessary for estimating ΔT_{stat}. To minimise P_e, the cell is thermally isolated in vacuum and surrounded by a thermal shield (environment) controlled to a temperature T_e close to the cell temperature T_c.

The magnitude of R_{cs} depends strongly on the cell geometry, which influences the mean thickness and the area of the liquid layer formed between the metallic body and the solid phase. This mean thickness, and thus R_{cs}, may increase significantly with rising fraction F of sample melted, i.e. especially temperature values measured at the end of a melting experiment may deviate significantly from the equilibrium curve $T_s(F)$ due to heat leaks.

If the heat load P_u is sufficiently small, the difference ΔT_{cs} is nearly constant under steady-state conditions because the relative change of the mean liquid-layer thickness with time is small. If the power is too large during heating, steady-state conditions cannot be reached and a reliable determination of R_{cs} applying Equation (1) is not possible. In most cases, the second situation occurs during the heat pulses used for measuring the melting curves by the intermittent-heating method. Thus, small additional heat pulses have to be used, for which the small heating power is adjusted in such a way that the overheating can be measured sufficiently accurately, but steady-state conditions (no significant change of ΔT_{cs} with time) are nearly reached and ΔT_{cs} depends linearly on the heating power.

The determination of R_{cs} depends on the position of the heater. Ideally, the heater should be located so that it feeds the heat nearly into a path resulting in realistic overheating as would be caused by the heat load, i.e. yielding a reliable maximum estimation of ΔT_{stat} by $P_u R_{cs}$. However, in most cases, the fraction of the heat load influencing the thermometer reading and its path are unknown. Therefore, a correction of the error ΔT_{stat} is impossible and a worst case scenario has to be assumed in the uncertainty estimate. If R_{cs} has been determined appropriately, the following relation is approximately fulfilled [Wolber and Fellmuth 2011]:

$$\Delta T_{stat}/\Delta T_e \approx R_{cs}/R_e , \qquad (2)$$

where ΔT_e is a change of T_e and R_e is the total thermal isolation resistance between the cell and its environment. (This simple relation only holds for sufficiently large isolation resistances R_e, i.e.

approaching adiabatic conditions. Otherwise the solution looks much more complicated [Wolber and Fellmuth 2011]. One method for determining R_e is to observe the change of the cell-temperature drift due to a jump of the temperature of its environment.) Using Equation (2) for checking purposes, it has to be considered that it may be necessary to wait a long time period (one hour or more) until the shield has become sufficiently isothermal after a temperature jump. (Temperature gradients on the shield may be monitored by the aid of differential thermocouples pasted on it.) A further overall check of the thermal conditions is possible by comparing the measured heat of fusion Q_{HF} with the value expected from the amount of fixed-point substance, when known.

One method for determining the heat load P_u is to measure the drift of the temperature of the cell dT_c/dt (t time) outside the melting range under nearly the same isothermal conditions as during the measurement of the melting curve. The expression $C_c\, dT_c/dt$ then gives the heat load P_u, where C_c is the heat capacity of the cell assembly. To check the stability of the measuring conditions, the drift has to be determined before and after the measurement of a melting curve. In both cases, T_c should deviate at least 10 mK from the melting temperature. This ensures that the effective heat capacity is not increased by pre-melting effects (below the melting range) or by the melting of the last small solid pieces (above the melting range), respectively. (For hydrogen cells, it might be necessary to investigate the temperature dependence of the heat capacity of the cell in a range of 100 mK below the melting range or even larger due to the pre-melting caused by the spin-conversion catalyst [Fellmuth *et al.* 2005].)

3.3   Recovery periods and dynamic temperature-measurement errors

The dynamic behaviour of a cell determines the thermal recovery after a heat pulse. This thermal recovery may deviate significantly from a simple exponential law with one time constant τ. Nevertheless, it is convenient to characterize the order of magnitude of the minimum recovery time period $t_{r,min}$ required to attain thermal equilibrium by a time constant. For a simple RC model, the relation $\tau_{RC} = R_{cs}\, C_{cw}$ is approximately valid, with C_{cw} being the heat capacity of the metallic parts (wall) of the cell. $t_{r,min}$ can be estimated roughly applying the relation $t_{r,min} = \tau_{RC} \ln(\Delta T_{cs,pulse}/\Delta T_{dyn,max})$, where $\Delta T_{cs,pulse}$ is the initial overheating after a heat pulse and $\Delta T_{dyn,max}$ is the maximum allowed dynamic error $\Delta T_{dyn} = T_c - T_{c,equ}$ ($T_{c,equ}$ is the equilibrium temperature of the cell).

But the simple RC model holds only for the relatively quick first recovery of the metallic body of the cell with respect to the adjacent layer of liquid phase (for details see [Fellmuth and Wolber 2011]). In most cases a second part of the recovery is observed, where thermal equilibrium is reached in different portions of the fixed-point sample itself and in the cell body. This equalizing process may last much longer than the first exponential one. It is, therefore, dangerous to estimate the overall necessary recovery period from the magnitude of the time constant τ_{RC}. As a basis for measuring $T_s(F)$ at the highest level of accuracy, dedicated experiments are necessary providing at least once sufficient post-pulse recovery times (may be several hours) until the true equilibrium temperature is definitely reached. Since R_{cs} and thus the thermal conditions depend on F, the experiments have to be performed in the whole F range of interest. From these experiments, the recovery periods $t_{r,\Delta T}$ can be derived that are necessary to obtain a desired level of the dynamic error $\Delta T = \Delta T_{dyn,max}$. Contrary to a time constant, the recovery period $t_{r,\Delta T}$ depends on the overheating at the end of the heat pulse. Since the time dependence of ΔT_{dyn} may be complicated, it is not possible to specify a limit for the remaining drift as an alternative criterion. In some cases, especially with Ne cells, it turned out practically impossible to wait sufficiently long. A model explaining these extreme long recovery periods is described in [Wolber and Fellmuth 2008, 2011 and 2013, Fellmuth and Wolber 2011]). In

such cases, a remedy may be to find the asymptotic value T_{equ} by fitting the thermal recovery by a superposition of exponential components.

3.4   Determination of the liquidus-point temperature

The liquidus point (infinitesimal amount of solid phase, i.e. fraction F of sample melted practically equal to one) is considered to be the best approximation of the triple-point temperature for a given fixed-point sample. This approach follows from the fact that the influences of crystal defects and impurities having equilibrium distribution coefficients smaller than one on the melting temperature decreases with increasing F. Furthermore, the liquidus point is the only point on a phase-transition curve amenable to modelling concerning the influence of impurities, see ITS-90 *Guide* *Influence of Impurities*.

Since measurements up to $F = 1$ are not possible, $T_s(F=1)$ has to be obtained by some sort of extrapolation of the melting curve. It should be noted that the temperature T_w of the sensor element (wire) differs from T_s due to the so-called "self-heating" and ΔT_{stat}. Since ΔT_{stat} depends on R_{cs}, the dependence $R_{cs}(F)$ may influence the shape of the observed melting curve. Especially if R_{cs} becomes larger than 1 K/W, it may become necessary to determine both the "self-heating" and $R_{cs}(F)$ not only at one F value, but in detail as a function of F. This demand results from the fact that R_{cs} is not very small compared with the internal thermal resistance of the thermometer (of order 100 K/W). (A method for deducing the liquidus temperature $T_{LP} = T_s(F=1)$ from $T_w(F)$ is described in [Wolber and Fellmuth 2011 and 2013]. This method is based on generalized thermal models.) Thus, a careful analysis of the static temperature-measurement error depending on F is of crucial importance to obtain the lowest uncertainties.

The extrapolation is done by fitting a function $T_{obs}(F)$ to the experimental data, keeping in mind the following suggestions:

- The fitting should be performed in an F range for which the melting temperature of the fixed-point sample can be determined with the lowest possible uncertainty. Most physical effects influence the melting temperature at low F values where the solid phase dominates (i.e. effects arising from the influence of crystal defects, of the spin-conversion catalyst necessary to realize the triple-point of equilibrium hydrogen, etc.). On the other hand, the melting curves become more sensitive to the thermal surroundings as melting proceeds towards large F values. Thus, the choice of the F range used for fitting should be considered very carefully after taking into account the properties and behaviour of the specific fixed-point material.
- The form of the function $T_{obs}(F)$ should correspond to the F-dependence of the effects influencing the shape of the melting curve. (The simplest approaches are to fit T_{obs} versus F or $1/F$.) The choice should be guided by selecting a form that minimizes the standard deviation of the experimental data from the fit function and maximizes the repeatability of the liquidus-point temperature.

4   ANALYSIS OF PERFORMANCE AND ESTIMATION OF UNCERTAINTY

4.1   Effects influencing the melting curves and properties of the fixed-point substances

For evaluating the observed melting curves and estimating reliably the uncertainty of the realized triple-point temperature, it is crucial to consider the different effects influencing the shape and temperature of the melting curve depending on the universal and specific properties of the cryogenic gases as fixed-point substances (e.g. influence of crystal defects and the freezing conditions including refreezing). (Universal and specific properties are summarised in [Fellmuth and Wolber 2011].) A comprehensive knowledge could be gained in the framework of two connected international intercomparisons of sealed cells [Pavese *et al.* 1984, Pavese 1984, Fellmuth *et al.* 2012] together with two international collaborations directed to the investigation of isotopic effects in hydrogen [Fellmuth *et al.* 2005] and neon [Steur *et al.* 2015]. This was possible because the included cells were quite different with respect to their design, materials, and preparation as well as to the source and purity of the gas sample and the filling technology and date, which allowed separation of the different effects. First of all, in accordance with the estimation performed in [Liu *et al.* 1992], the results obtained demonstrate a high long-term stability of the triple-point temperatures since they are not clearly correlated with the cell age. Dedicated investigations were performed concerning the influence of the freezing and annealing conditions on the thermal recovery, the internal thermal resistance and the shape of the equilibrium melting curves, especially for neon cells [Wolber and Fellmuth 2008 and 2011]

All melting curves are depressed at the beginning. This is suspected to be caused primarily by the influence of crystal defects. The distorted sample parts melt at lower temperatures due to the weakening of the crystal lattice, which results in smaller binding energies. This effect is called pre-melting. The usually observed long creeping in the recovery at low F values supports this hypothesis. (In [Wolber and Fellmuth 2011] it is explained why extremely long time periods may be necessary for the thermal recovery after the pulses of the intermittent heating used for the calorimetric method if the melting temperature is macroscopically inhomogeneous within the sample.)

The specific properties of the four fixed-point substances have the following influence on the melting curves:

➢ Hydrogen: Depending on the amount of the spin-conversion catalyst, the pre-melting of sample portions in direct contact with the catalyst significantly influences the beginning of the melting curves. (The possible causes of the melting-temperature depression by the catalyst and dedicated investigations of this effect are discussed in [Fellmuth *et al.* 2005].) But in the region where the melting temperature is not influenced by the catalyst, the melting curves are typically very flat. This flat part of the curves is often called "plateau". Since the width of the temperature range covered by the plateau is usually less than 0.1 mK, the "natural width" of the melting range of high-purity, undistorted solid hydrogen is at most 0.1 mK. In view of the effect of the deuterium concentration, this means that usually the redistribution of the two isotopes during freezing and melting is very small. (The redistribution is governed by the distribution coefficient and the freezing conditions.)

➢ Neon: The many melting curves of neon samples measured in the second international intercomparison of sealed cells [Fellmuth *et al.* 2012] with vanishingly small heat loads are almost all sloped upwards to the highest fractions of sample melted F. One possible explanation could be the isotopic redistribution, which takes place both macroscopically during freezing and microscopically during melting. The fact that macroscopic redistribution depends on the freezing conditions may be one cause for observing quite different slopes of the melting curves. The

freezing conditions are of course influenced by the design of the cells. Above about $F = 30\%$, the melting curves are often nearly straight lines in the representation versus F, whereas the $1/F$ representation would yield a typical strong curvature near $F = 100\%$. In this F range, the typical temperature width amounts to $(0.1 – 0.2)$ mK.

➤ Oxygen: After the depressed beginning, the melting curves of oxygen samples are typically very flat with temperature widths of only a few tens of microkelvins. This is comparable with the behaviour of hydrogen in the region where the melting temperature is not influenced by the catalyst. It indicates that the effect of crystal defects is relatively small. The flat melting curves are especially remarkable for those cells for which the large supercooling causes a quick freeze during the recalescence that extends throughout large portions of the fixed-point sample or even the whole sample. (Oxygen melts may supercool more than 1 K [Fellmuth and Wolber 2011].) For the effect of argon in oxygen on the shape and the temperature of the phase transition see next subsection.

➤ Argon: For argon samples, the melting curves may also be very flat at high F values, but often a slope near to the liquidus point has been found. Apart from the influence of impurities, which should be sufficiently small for state-of-the-art high-purity argon, crystal defects seem to influence large portions of the melting curves after quick freezing. In [Sakurai 1999, Nakano *et al.* 2003 and 2007] it has been shown that a re-freezing substantially reduces the melting range. The re-freezing improves the crystal quality because it avoids the fast freezing of a large fraction of the sample after the supercooling [Fellmuth and Wolber 2011]. In accordance with this result, it has been found that partial re-freezing reduces the depression at the onset of the melt. On the other hand, a long annealing only a few millikelvin below the melting temperature has no effect. The possible influence of crystal defects on the melting temperature decreases with increasing F.

Fortunately, the melting curves of high-purity fixed-point samples are in many cases sufficiently flat and/or linear that detailed fitting is not necessary.

4.2 Uncertainty of the fixed-point realization

As one of the most important outcomes of the international intercomparisons and collaborations, considering the experience gained, agreement could be reached on how to estimate the uncertainty of the realization of the cryogenic fixed points, see [Pavese *et al.* 1984, Pavese 1984, Pavese *et al.* 2003a and 2010, Fellmuth *et al.* 2005, Fellmuth *et al.* 2012, Fellmuth 2013, Wolber and Fellmuth 2013, Steur *et al.* 2015]. The uncertainty budgets given in Table 2 illustrate the highest level. They are based on a linear model of the measurement and assume the application of the best equipment available. The components are arranged regarding their physical causes. They contain Type A and Type B parts. It should be emphasized that all components are dominated by physical effects, i.e. they cannot be reduced significantly by measuring many melting curves under the same conditions:

u_{imp} The estimate for the shift of the liquidus-point temperature by impurities considers the modern availability of hydrogen, oxygen, and argon gases with less than one part per million total impurity content (purity 99.9999 %). (The effect of argon contamination in oxygen is an insidious one as it has no effect on the melting range, see [Steur *et al.* 2017]. In the past, the manufacturer's specifications for argon content were frequently wrong by as much as an order of magnitude. This problem no longer exists nowadays, but an explicit assay is necessary.) Commercially available neon gases have a best purity of 99.9995 %. The data necessary for

estimating the shift applying the SIE (sum of individual estimates) method are given in ITS-90 *Guide* Section 2.1 *Influence of Impurities*.

u_{iso} In the Technical Annex of the *mise en pratique* of the definition of the kelvin (*MeP*-K) [Fellmuth *et al.* 2016, https://www.bipm.org/en/publications/mises-en-pratique] it is prescribed that for hydrogen samples the triple-point temperature has to be corrected to the Standard Light Antarctic Precipitation (SLAP) isotopic composition, and for neon to the IUPAC (International Union of Pure and Applied Chemistry) isotopic composition. It has been estimated that the uncertainty of the necessary correction is at most 20 µK for hydrogen [Fellmuth *et al.* 2005] and 4 µK for neon [Steur *et al.* 2015] applying state-of-the-art analysis techniques.

u_R The uncertainty of the resistance measurement is deduced from the parameters of the measuring devices used and the results of the comparison of ac and dc bridges. It includes the uncertainty of the "self-heating" correction.

u_{HC} The so-called head correction has to be applied since the sensor element of the thermometer cannot be located at the surface of the solid and liquid sample portions, where the three phases are in contact. It considers the hydrostatic pressure within the fixed-point cell. The estimation of this uncertainty component is complicated by the fact that the location of the sample within the cell is not definitely known, the thermometer measures an average temperature over a significant height, the midpoint of which is also not well known, and the metallic thermometer block smoothes out the temperature gradient. The values in Table 2 result from the data in Table 1 for an uncertainty of the immersion depth of 5 mm.

u_{stab} The short-term thermometer instability has been checked during the second international intercomparison of sealed cells [Fellmuth *et al.* 2012] by using at least three thermometers. The check is limited by the resolution of the devices. (It should be emphasised that the estimates given in Table 2 are realistic only for thermometers having an extremely high stability. At the triple point of hydrogen, rhodium-iron resistance thermometers are preferably used for cell comparisons because of the very small sensitivity of platinum resistance thermometers.)

u_{stat} The estimate for the static temperature-measurement error ΔT_{stat} is a measure for the quality of the calorimetry. It has been obtained using the methodology described in Subsection 3.2. For a typical value of the internal thermal resistance R_{cs} of the cell of 1 K/W, $\Delta T_{stat} = 10$ µK corresponds to a heat leak of 10 µW.

u_{dyn} The limits for dynamic temperature-measurement errors have been estimated considering the results of dedicated measurements performed with extremely long recovery periods after the heat pulses (several hours). This is especially important for neon cells, see for instance [Wolber and Fellmuth 2011].

u_{LP} The extrapolation to the liquidus point contributes to the uncertainty especially due to the scattering of the temperature values on the melting curve and the possible deformation of the measured shape of the curve mentioned in Subsection 3.4.

u_{rep} This repeatability component considers the influence of the preparation of the fixed-point sample with correspondingly varying melting-curve shapes. This component has been estimated from the results of dedicated experiments, in which the freezing and experimental conditions were varied considerably.

u_{cnsi} For hydrogen samples, an additional uncertainty component is caused by the necessary conversion to the equilibrium composition of the two nuclear-spin isomers. This conversion has been investigated within the framework of an international collaboration [Fellmuth *et al.* 2005].

Table 2. Highest-level uncertainty budgets for the realization of the defining cryogenic fixed points of the ITS-90. The estimates are based on the results of international intercomparisons and collaborations, see [Pavese *et al.* 1984, Pavese 1984, Pavese *et al.* 2003a and 2010, Fellmuth *et al.* 2005, Fellmuth *et al.* 2012, Fellmuth 2013, Wolber and Fellmuth 2013, Steur *et al.* 2015]. The estimated values are given in μK.

Symbol	Component	Hydrogen	Neon	Oxygen	Argon
u_{imp}	Shift of the LP temperature by impurities	11	35	22	22
u_{iso}	Correction of the isotopic composition	20	4		
u_R	Resistance measurement	10	10	10	10
u_{HC}	Head correction	1	10	8	17
u_{stab}	Short-term thermometer instability	8	8	8	8
u_{stat}	Static temperature-measurement error	10	10	10	10
u_{dyn}	Dynamic temperature-measurement error	10	15	10	15
u_{LP}	Extrapolation to the liquidus point (LP)	8	15	8	12
u_{rep}	Repeatability of T_{LP} due to sample properties	5	15	5	12
u_{cnsi}	Composition of nuclear-spin isomers	10			
u_{comb}	**Combined standard uncertainty**	**33**	**48**	**32**	**39**

The order of magnitude of the estimates given in Table 2 is impressively supported by the conclusions of the second international intercomparison of sealed cells [Fellmuth *et al.* 2012], which are based on a huge amount of data for quite different cells: "The state-of-the-art level of accuracy of the fixed-point realizations was estimated by the standard deviations of the liquidus-point melting temperatures, obtained by extrapolation of the melting curves, of sealed cells filled with gases having nominal purities of 99.999% or better: 30 μK (hydrogen after correcting for the influence of the deuterium content), 89 μK (neon uncorrected for the effect of the variability of the isotopic composition in samples prepared from air), 57 μK (oxygen), and 58 μK (argon)." (Table 2 is also supported by the results of the first international intercomparison of fixed points by means of sealed cells [Pavese *et al.* 1984, Pavese 1984] and two CIPM Key Comparisons [Steele *et al.* 2002, Rusby *et al.* 2006]. But the uncertainty level is much larger because the data depend on the stability of the thermometers used as transfer standards.) For neon, the situation is now much improved due to the correction procedures prescribed in the Technical Annex of the *mise en pratique* of the definition of the kelvin (*MeP*-K) [Fellmuth *et al.* 2016, https://www.bipm.org/en/publications/mises-en-pratique]. In accordance with the estimates for u_{imp}, the liquidus-point temperatures were not significantly correlated with purity for samples having a nominal purity of 99.999 % or better. In summary, it can be stated that a realization of the cryogenic fixed points with standard uncertainties of better than 0.1 mK can be achieved applying modern high-purity gases and state-of-the-art techniques.

References

Ancsin J., Phillips J. 1969 Triple point of argon, *Metrologia* **5**, 77-80

Ancsin J. 1970 The Triple Point of Oxygen and its Change be Noble Gas Impurities, *Metrologia* **6**, 53-56

Ancsin J. 1973a Dew Points, Boiling Points and Triple Points of "Pure" and Impure Oxygen, *Metrologia* **9**, 26-39

Ancsin J. 1973b Studies of Phase Changes in Argon, *Metrologia* **9**, 147-154

Ancsin J., Phillips J. 1976 Argon Triple Point Realization Cryostat for Platinum Resistance Long Stem Thermometers, *Rev. Sci. Instr.* **47**, 1519-1521

Ancsin J. 1978 Intercomparison of Triple Points of Argon and Oxygen of INM, IMGC and NRC, *Metrologia* **14**, 79-81

Bloembergen P., Bonnier G., Ronsin H. 1990 An International Intercomparison of Argon Triple Point Calibration Facilities, Accommodating Long-stem Thermometers, *Metrologia* **27**, 101-106

Bonnier G. 1975 Point triple de l'argon (83,798 K) référence de transfert, *Bulletin du Bureau National de Métrologie* **22**, 14-18

Bonnier G., Malassis R. 1975 Réalisation d'un nouveau type de cellule scellée destinée aux étalonnages cryogéniques, *Bulletin du Bureau National de Métrologie* **22**, 19-20

Bonnier G. 1987 Calibration of Temperature Sensors, *Proc. 3rd International Symposium on Temperature and Thermal Measurements in Industry and Science* (TEMPMEKO '87), (Institute of Measurement and Control, London), pp. 57-68

Compton J.P., Ward S.D. 1976 Realization of the Boiling and Triple Points of Oxygen, *Metrologia* **12**, 101-113

Consultative Committee for Thermometry (CCT) 2010 Estimates of the Differences between Thermodynamic Temperature and the ITS-90, http://www.bipm.org/utils/common/pdf/ITS-90/Estimates_Differences_T-T90_2010.pdf

Didi-Alaoui I., Fiorillo D., Vergé A., Sparasci F., Jouin D., Hermier Y. 2013 Design and Implementation of a Dedicated Calorimeter for Long Stem SPRTs Calibrations at the Argon and Oxygen Triple Points, *Proc. Temperature: Its Measurement and Control in Science and Industry*, Vol. 8, Ed. C.W. Meyer (AIP, Melville, New York) pp. 474-479

Ding R., Zhao M.J., Nerdrum E., Meier D. 2011 Development of the Triple-Point-of-Argon System, *Int. J. Thermophys.* **32**, 2252-2260

Ding R., Zhao M.J., Nielson T., Nerdrum E., Farley D. 2012 Experimental Study and Computer Modeling of the Triple Point of Argon System, *NCSLI Measure* **7**, 58-62

Fellmuth B., Seifert P., Rudloff H. 1997 Realisation of low-temperature fixed-points, *Proc. 6th International Symposium on Temperature and Thermal Measurements in Industry and Science* (TEMPMEKO '99), Ed. P. Marcarino (Levrotto & Bella, Torino) pp. 93-98

Fellmuth B., Berger D., Wolber L. 1999 An international star intercomparison of low-temperature fixed points using sealed triple-point cells, *Proc. 7th International Symposium on Temperature and Thermal Measurements in Industry and Science* (TEMPMEKO '99), Ed. J.F. Dubbeldam, M.J. de Groot (IMEKO / NMi Van Swinden Laboratorium, Delft) pp. 233-238

Fellmuth B., Wolber L., Hermier Y., Pavese F., Steur P.P.M., Peroni I., Szmyrka-Grzebyk A., Lipinski L., Tew W.L., Nakano T., Sakurai H., Tamura O., Head D., Hill K.D., Steele A.G. 2005 Isotopic and other influences on the realization of the triple point of hydrogen, *Metrologia* **42**, 171-193

Fellmuth B., Wolber L. 2011 Investigation of the Parameters of Sealed Triple-Point Cells for Cryogenic Gases, *Int. J. Thermophys.* **32**, 161-172

Fellmuth B., Wolber L., Head D.I., Hermier Y., Hill K.D., Nakano T., Pavese F., Peruzzi A., Rusby R.L., Shkraba V., Steele A.G., Steur P.P.M., Szmyrka-Grzebyk A., Tew W.L.,

Wang L., White D.R. 2012 Investigation of low-temperature fixed points by an international star intercomparison of sealed triple-point cells, *Metrologia* **49**, 257-265

Fellmuth B. 2013 New Protocol For The Realization Of The Triple Points Of Cryogenic Gases As Temperature Fixed Points, *Proc. Temperature: Its Measurement and Control in Science and Industry*, Vol. 8, Ed. C.W. Meyer (AIP, Melville, New York) pp. 174-179

Fellmuth B., Fischer J., Machin G., Picard S., Steur P.P.M., Tamura O., White D.R., Yoon H. 2016 The kelvin redefinition and its *mise en pratique*, *Phil. Trans. R. Soc.* A **374**, 20150037, http://rsta.royalsocietypublishing.org/content/roypta/374/2064/20150037, DOI: 10.1098/rsta.2015.0037, Published 22 February 2016

Fischer J., Wolber L., de Podesta M., Rusby R., Hill K.D. Moldover M., Pitre L., Steur P., Tamura O., White R. 2011 Present estimates of the differences between thermodynamic temperatures and the ITS-90, *Int. J. Thermophys.* **32**, 12-25 (Proc. of TEMPMEKO 2010)

Furukawa G.T. 1992 Argon triple point apparatus with multiple thermometer wells, *Proc. Temperature, Its Measurement and Control in Science and Industry*, Vol. 6, Ed. J.F Schooley (AIP, New York) pp. 265-269

Hermier Y, Pitre L., Geneville C., Vergé A., Bonnier G., Head D.I., Fellmuth B., Wolber L., Szmyrka-Grzebyk A., Lipinski L., de Groot M.J., Peruzzi A. 2003 A New Generation of Multicells for Cryogenic Fixed Points at BNM/INM, *Proc. Temperature: Its Measurement and Control in Science and Industry*, Vol. 7, Ed. D.C. Ripple *et al.* (AIP, Melville, New York) pp. 179-184

Hermier Y., Bonnier G., Chimenti V., del Campo D., Tichy M., Marcarino P., Steur P.P.M., Dematteis R., Filipe E., Rauta C., de Groot M.J., Nielsen J., Bruce S., Head D., Rusby R., Steiner A., Weckström T., Fellmuth B., Thiele-Krivoj B., Bojkovski J., Ivarsson J., Kalemci M., Ugur S. 2005 Intercomparison of argon triple-point cells in the frame of EUROMET Project No.502 *Proceedings 9th International Symposium on Temperature and Thermal Measurements in Industry and Science* (TEMPMEKO 2004), Ed. D. Zvizdic, L.G. Bermanec, T. Veliki and T. Stašic (IMEKO / University of Zagreb, Faculty of Mechanical Engineering and Naval Architecture, Zagreb) ISBN 953-6313-71-5, pp. 1037-1042

Hill K.D., Steele A.G. 2003 The Non-Uniqueness of the ITS-90: 13.8033 K to 273.16 K, *Proc. Temperature: Its Measurement and Control in Science and Industry*, Vol. 7, Ed. D.C. Ripple *et al.* (AIP, Melville, New York) pp. 53-58

Kemp R.C., Kemp W.R.G., Cowan J.A. 1976 The Boiling Points and Triple Points of Oxygen and Argon, *Metrologia* **12**, 93-100 http://iopscience.iop.org/article/10.1088/0026-1394/12/3/002

Liu F., Yang W., Huang N. 1992 A study of the preparation of sealed cells for thermometry, *Proc. Temperature: Its Measurement and Control in Science and Industry*, Vol. 6, Ed. J.F. Schooley (AIP, New York) pp. 257-260

Nakano T., Tamura O., Sakurai H. 2003 New Sealed Cells for Realization of Cryogenic Fixed Points at NMIJ/AIST, *Proc. Temperature: Its Measurement and Control in Science and Industry*, Vol. 7, Ed. D.C. Ripple *et al.* (AIP, Melville, New York) pp. 185-190

Nakano T., Tamura O., Sakurai H. 2007 Realization of Low-Temperature Fixed Points of the ITS-90 at NMIJ/AIST, *Int. J. Thermophys.* **28**, 1893-1903

Pavese F., Cagna G., Ferri D. 1976 Miniature sealed cells as an easy-to-use temperature calibration device and a precision thermostat for cryogenic temperatures *Proc. VI International Cryogenic Engineering Conference (ICEC 6)* (IPC Science and Technology Press, Guildford) pp. 205-207

Pavese F., Demonti G., Ferri D. 1978 Alternate sets of fixed points for simplified realisations of IPTS-68 *Advances in Cryogenic Engineering,* Vol. **23**, Ed. K.D. Timmerhaus (Plenum Press, New York, London) pp. 503-511

Pavese F. 1978 The triple point of argon and oxygen, *Metrologia* **14**, 93-103

Pavese F. (ed) 1984 *International intercomparison of fixed points by means of sealed cells (13.81 K to 90.686 K) BIPM Monograph* 84/4 (Bureau International des Poids et Mesures, Sèvres)

Pavese F., Ancsin J., Astrov D.N., Bonhoure J., Bonnier G., Furukawa G.T., Kemp R.C., Maas H., Rusby R.L., Sakurai H., Ling Shan-Kang 1984 An International Intercomparison of Fixed Points by Means of Sealed Cells in the Range 13.81 K-90.686 K, *Metrologia* **20**, 127-144 http://iopscience.iop.org/article/10.1088/0026-1394/20/4/002

Pavese F., Fellmuth B., Head D., Hermier Y., Peruzzi A., Szmyrka-Grzebyk A., Zanin L.2003a "MULTICELLS": A European Project On Cryogenic Temperature Fixed Points In Sealed Cells, *Proc. Temperature: Its Measurement and Control in Science and Industry*, Vol. 7, Ed. D.C. Ripple *et al.* (AIP, Melville, New York) pp 161-166

Pavese F., Ferri D., Peroni I., Pugliese A., Steur P.P.M., Fellmuth B., Head D., Lipinski L., Peruzzi A., Szmyrka-Grzebyk A., Wolber L. 2003b Cryogenic Temperature Sealed Fixed Points: IMGC New-Generation of Modular Cells, *Proc. Temperature: Its Measurement and Control in Science and Industry*, Vol. 7, Ed. D.C. Ripple *et al.* (AIP, Melville, New York) pp 173-178

Pavese F., Steur P.P.M., Bancone N., Ferri D., Giraudi D. 2010 Comparison with $U \approx 50$ μK of neon samples of different isotopic compositions, *Metrologia* **47**, 499–517

Pavese F., Steur P.P.M., Jin Seog Kim, Giraudi D. 2011 Further results on the triple point temperature of pure ^{20}Ne and ^{22}Ne, *J. Chem. Thermodyn.* **43**, 1977-1983

Pavese F., Molinar Min Beciet G. 2013 *Modern Gas-Based Temperature and Pressure Measurements* (Springer Science + Business Media, New York)

Pond S.L. 2003 Argon Triple-Point Apparatus for SPRT Calibration, *Proc. Temperature: Its Measurement and Control in Science and Industry*, Vol. 7, Ed. D.C. Ripple *et al.* (AIP, Melville, New York) pp 203-208

Preston-Thomas H. 1990 The International Temperature Scale of 1990 (ITS-90), *Metrologia* **27**, 3-10, 107

Rusby R., Head D., Meyer Ch., Tew W., Tamura O., Hill K.D., de Groot M., Storm A., Peruzzi A., Fellmuth B., Engert J., Astrov D., Dedikov Y., Kytin G. 2006 Final Report on CCT-K1: Realizations of the ITS-90, 0.65 K to 24.5561 K, using rhodium–iron resistance thermometers, *Metrologia* **43,** 03002

Sakurai H. 1999 Precise realization of the triple points of equilibrium hydrogen and argon using a closed cycle refrigerator, *Proc. 7th International Symposium on Temperature and Thermal Measurements in Industry and Science* (TEMPMEKO '99), Ed. J.F. Dubbeldam, M.J. de Groot (IMEKO / NMi Van Swinden Laboratorium, Delft) pp 124-128

Sakurai H. 2003 Calorimetric study of the triple point of equilibrium hydrogen, *Proc. 8th International Symposium on Temperature and Thermal Measurements in Industry and Science* (TEMPMEKO 2001), Ed. B. Fellmuth, J. Seidel, G. Scholz (VDE Verlag GmbH / Berlin) ISBN 3-8007-2676-9, pp. 411_416

Sparasci F., Pitre L., Rouillé G., Thermeau J.-P., Truong D., Galet F., Hermier Y. 2011 An Adiabatic Calorimeter for the Realization of the ITS-90 in the Cryogenic Range at the LNE-CNAM, *Int. J. Thermophys.* **32**, 201-214

Steele A.G. 1997 Fixed-point cryostat using closed-cycle refrigerator: Design and control, *Proc. International Seminar on Low Temperature Thermometry and Dynamic Temperature Measurement*, Ed. A. Szmyrka-Grzebyk (DRUK, Wrocław) pp. L48-L53

Steele A.G., Fellmuth B., Head D.I., Hermier Y., Kang K.H., Steur P.P.M., Tew W.L. 2002 CCT-K2: Key Comparison of Capsule-type Standard Platinum Resistance Thermometers from 13.8 K to 273.16 K, *Metrologia* **39**, 551-571

Steur P.P.M., Pavese F., Fellmuth B., Hermier Y., Hill K.D., Kim J.S., Lipinski L., Nagao K., Nakano T., Peruzzi A., Sparasci F., Szmyrka-Grzebyk A., Tamura O., Tew W.L., Valkiers S., van Geel J. 2015 Isotopic effects in the neon fixed point: Uncertainty of the calibration data correction, *Metrologia* **52**, 104-110

Steur P.P.M., Yang I., Pavese F. 2017 Evidence for Argon Content in Pure Oxygen from Thermal Data *Int. J. Thermophys.* **38**(2):20, DOI 10.1007/s10765-016-2160-z

Wolber L., Fellmuth B. 2008 Influence of the Freezing and Annealing Conditions on the Realisation of Cryogenic Triple Points, *Int. J. Thermophys.* **29**, 82-92

Wolber L., Fellmuth B. 2011 Improved Thermal Model for the Realization of the Triple Points of Cryogenic Gases as Temperature Fixed Points, *Int. J. Thermophys.* **32**, 189-200

Wolber L., Fellmuth B. 2013 *Star intercomparison of sealed triple-point cells filled with cryogenic gases. Part I: Protocol* (PTB, Braunschweig) ISBN 978-3-95606-046-5

Yang I., Song C.H., Kim Y.-G., Gam K.S. 2011 Cryostat for Fixed-Point Calibration of Capsule-Type SPRTs, *Int. J. Thermophys.* **32**, 2351-2359

APPENDICES

Appendix 1 *Suggested Measurements and Measurement Conditions*

Appendix 2 *Recorded Data*